

# MICROSTRUCTURE AND MECHANICAL PROPERTIES OF SLAG ACTIVATED WITH SODIUM SILICATE

RICHARD CARON and FRANK DEHN

*Building Materials and Concrete Construction, MPA Karlsruhe, Karlsruhe Institute of Technology (KIT), Karlsruhe, Germany*

The study focuses on developing a detailed understanding of microstructure and mechanical behaviour of alkali-activated slag with sodium silicate. The slag used in this study was provided by Ecocem (Netherlands) and consists of 38.8 % CaO, 36.3 % SiO<sub>2</sub>, 12.8 % Al<sub>2</sub>O<sub>3</sub> and 8.0 % MgO. It was activated with two sodium silicate solutions. The two mixes were studied on a paste level. They have the same water/slag ratio  $w/s = 0.4$  kg/kg and the same sodium content  $n = 5.0$  g Na<sub>2</sub>O / 100 g slag. Two silicate ratios were investigated:  $M_s = 0.5$  and  $M_s = 2.2$  moles of SiO<sub>2</sub> / moles of Na<sub>2</sub>O. Early-age mechanisms and reaction products of the activation of the slag were analysed with isothermal calorimetry, SEM images and chemical characterization. In addition, compressive and flexural strength were determined. Despite different reaction steps in comparison to ordinary Portland cement, the obtained mechanical properties seem to be sufficient for structural application.

*Keywords:* Activation, Kinetics, Compressive strength, Structural applications.

## 1 INTRODUCTION

Slag is a by-product of the steel industry, which can be used as a precursor when it is mixed with alkali solutions like sodium silicate. In comparison to the hydration of cement, activation of slag with sodium silicate presents two acceleration periods (Shi and Day 1995). Isothermal calorimetry curves for hydration of ordinary Portland cement (OPC) have already been interpreted in terms of competing parallel single-particle models (Parrot and Killoh 1984). The reaction products of alkali-activated slag (AAS) are different from OPC. C-A-S-H, hydrotalcite-type phases and ettringite are the main products reported in the literature (Haha *et al.* 2011, Myers *et al.* 2015, Gong and White 2016, Prentice *et al.* 2018). Nevertheless, compressive strength and flexural strength of such binders were proved to be reasonable for structural applications (Fernández-Jiménez and Puertas 2003). Extension of the interpretation of isothermal calorimetry, chemical characterization of AAS paste and determination of strength are included in this contribution.

## 2 MATERIAL, METHODS AND MODELING

### 2.1 Materials

The slag used in this study comes from the Dutch company Ecocem. Its oxide composition was analyzed by X-Ray Fluorescence with a M4 Tornado (Brucker GmbH Karlsruhe Germany) and is given in Table 1. Sodium silicate solutions were obtained by mixing three components: a first

solution composed at 50 % in mass of NaOH; a waterglass solution commercialized by Woellner (Betol 39T of solute concentration 34.5 % with a molar ratio  $M_{S,raw} = 3.4 \text{ SiO}_2 / \text{Na}_2\text{O}$  [mol/mol]); finally, distilled water was added to reach the correct water/slag ratio  $w/s = 0.4$  [kg/kg]. Two solutions were studied. They have both the same sodium content  $n = 5.0$  [g  $\text{Na}_2\text{O}$  / 100 g slag], but two different silicate ratios  $M_S = \text{SiO}_2/\text{Na}_2\text{O}$ . The mix named mix 1S has  $M_S=0.5$  [mol/mol], while the mix named mix hS has  $M_S = 2.2$  [mol/mol]. These molar ratios were chosen after an experimental campaign on different  $M_S$ . Receipts with intermediate  $M_S$ , between 0.8 and 1.8 showed quick setting time, which is a problem for considering practical applications. The solutions were premixed one day before the first contact between the solution and the slag, to ensure temperature equilibrium of the solution. The materials were studied on a paste level at a temperature of 20 °C.

Table 1. Oxide composition of the raw slag.

Oxide	CaO	SiO <sub>2</sub>	Al <sub>2</sub> O <sub>3</sub>	MgO	Other
Mass (%)	38.8	36.3	12.8	8.0	4.1

## 2.2 Methods

To generate the paste, the mixing process last four minutes overall, with a break between 90 and 120 seconds. Reaction kinetics were measured with both calorimetry and scanning electron microscopy (SEM) technics. For the calorimetry analysis, an eight-channel TAM Air isothermal calorimetry (TA Instruments, USA) was used. Samples were mixed outside of the calorimeter and put in the calorimetry chamber less than five minutes after the beginning of the mix. Due to the opening of the calorimeter, the measured heat release is considered only after twenty minutes. The measurements last seven days. Parallel samples were cast, demolded after one day and covered in plastic bags. After 7, 28 and 56 days, some samples were crushed into particles with 2mm thickness. Their activations were stopped via the solvent exchange method with isopropanol following the indications from (Zhang and Scherer 2011). After these seven days, the samples were stored in a desiccator until analysis. Polishing and carbon coating was performed before being analyzed with a Hitachi benchtop ESEM TM3030. A magnification factor of 800x was used. Post-processing of the obtained images allows determining the proportion of unreacted slag since the corresponding pixels are brighter. From this result and the volume of unreacted slag in the system at the beginning of the mixing, the proportion of reacted slag can be determined.

Still with parallel specimens, chemical analysis of the pastes was performed after 28 days. X-Ray diffraction (XRD) analysis was carried out with a Bruker D8 Advance instrument with  $\text{Cu-K}\alpha$  radiation and a nickel filter. The  $2\theta$  angle range was  $[5^\circ ; 70^\circ]$ , the step size was  $0.02^\circ$  with 0.2 s between each step. Both differential thermogravimetry (DTG) and differential thermal analysis (DTA) were realized with a Netzsch Simultaneous Thermal Analysis STA 409 under a  $\text{N}_2$  atmosphere with samples of 100 mg. The gradient of  $10^\circ\text{C}/\text{min}$  was applied, between  $100^\circ\text{C}$  and  $1000^\circ\text{C}$ . Finally, Fourier-Transform Infrared Spectroscopy (FTIR) was made with a Bruker Tensor 27 IR on the range  $[600 \text{ cm}^{-1}; 4000 \text{ cm}^{-1}]$ . The resolution was  $1 \text{ cm}^{-1}$ .

Flexural and compressive strengths were determined on paste prisms of  $2 \times 2 \times 8 \text{ cm}^3$  after 1, 2, 3, 7, 28 and 56 days. The tests were performed following the standard DIN EN 196-1 (DIN EN 196-1 2016) with adapted loading rates: 10 N/s for flexural strength and 100 N/s for compressive strength. The choice of this geometry is justified by its easy implementation. It permits to have a first indication of the mechanical properties of the mixes before considering structural applications.

## 2.3 Modeling

Activation kinetics of slag was modeled with a succession of six steps, each step corresponding to a single particle model. The steps were identified from the isothermal calorimetry curve. The initial dissolution and wetting of slag are not considered in this model. The isothermal curve for AAS with sodium silicate is composed of two acceleration periods, corresponding to two peaks in the isothermal calorimetry curve (three if the initial dissolution and wetting of slag are taken into account). The degree of reaction from the isothermal calorimetry curve  $\alpha_{cal}$  is obtained as follows. Firstly, the cumulative heat release  $Q$  is extrapolated from the beginning of the second peak  $t_{st,2}$  with the exponential model proposed in Eq. (1) (Riding *et al.* 2012):

$$Q(t) = Q_{\infty} \exp\left(-\left[\frac{\tau}{t}\right]^{\beta}\right) \quad (1)$$

$\beta$ ,  $\tau$  and  $Q_{\infty}$  and are fitting parameters and  $Q_{max} = Q_{\infty} + Q(t = t_{st,2})$  the maximum heat release. Then,  $\alpha$  is defined as the ratio shown in Eq. (2):

$$\alpha_{cal}(t) = \frac{Q(t)}{Q_{max}} \quad (2)$$

Single-particle models are equations  $f_i$  linking the local degree of reaction  $\alpha_i$  with its derivative along with time  $d\alpha_i/dt$  by the reaction rate  $k_i$  as shown in Eq. (3):

$$f_i(\alpha_i) = \frac{1}{k_i} \frac{d\alpha_i}{dt} \quad (3)$$

The corresponding curve  $d\alpha_{cal}/dt$  in the function of  $\alpha_{cal}$  is built and decomposed in six steps. The increasing part of the first peak can be fitted with a nucleation model. Between this maximum and the end of the first peak, the reaction is modeled with a shrinking core process. The reaction between both peaks is the induction period, modeled with a zero-order reaction. The second peak is then modeled with the succession of a nucleation until the maximum, a shrinking core process and a diffusion process. The transition degree of reaction between the last shrinking core process and the diffusion process is chosen arbitrarily and corresponds to a clear change of slope in the heat flow curve. In the end, the global reaction model can be seen in Eq. (4):

$$\frac{d\alpha}{dt} = \sum_{i=1}^M (\alpha_{i,1} - \alpha_{i,0}) k_i f_i \left( \frac{\alpha - \alpha_{i,0}}{\alpha_{i,1} - \alpha_{i,0}} \right) Tr_i(\alpha, \alpha_{tr,i}) \quad (4)$$

where  $[\alpha_{i,0}; \alpha_{i,1}]$  defines the range of the  $i^{\text{th}}$  step,  $\alpha_{tr,i}$  corresponds to the transition from a step to another,  $Tr_i$  is the transition function between two steps. More details on the implementation are provided in (Caron *et al.* 2021).

SEM results are used to rescale  $\alpha_{cal}$  with the actual degree of dissolution of slag  $\alpha$  at 7 days. In addition, from the three measured degrees of reaction at 7, 28 and 56 days, the diffusion model is used and allows to predict the degree of reaction at later ages.

## 3 RESULTS AND DISCUSSION

### 3.1 Reaction Kinetics

Both heat flow and cumulative heat release obtained from isothermal calorimetry experiments are given in Figure 1. Both peaks occur earlier for the mix IS. The first peak is greater for the mix hS,

while the second peak is greater for the mix IS. The proposed model is calibrated and fitted for both mixes Figure 2. The good coefficient of determination, greater than 0.98 for both mixes, comfort the hypothesis of the succession of these governing-kinetic mechanisms.

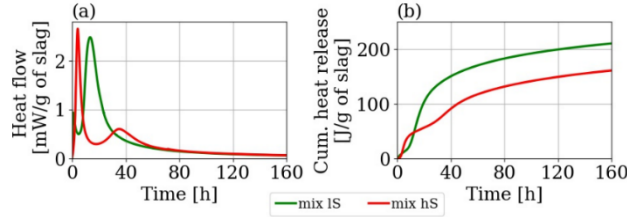


Figure 1. Isothermal calorimetry results: (a) heat flow and (b) cumulative heat release.

The first reaction process can be interpreted as a nucleation around the silicate crystals present from the beginning in the sodium silicate solution. This phenomenon would be comparable to what was found for alkali-activated fly ash (Lloyd *et al.* 2009). Then, the reaction is kinetically governed by a shrinking core process coming from the reduction of surface exchange between the pore solution and the slag particles. The second peak follows the same mechanisms as what was already proposed for OPC with the Parrot-Killoh model: nucleation occurs at the surface of the slag particle. Then, the reaction is controlled by the reduction of the surface of the slag particle. Finally, the reaction products form a barrier around the slag particle and the reaction is kinetically governed by the diffusion of ions through it.

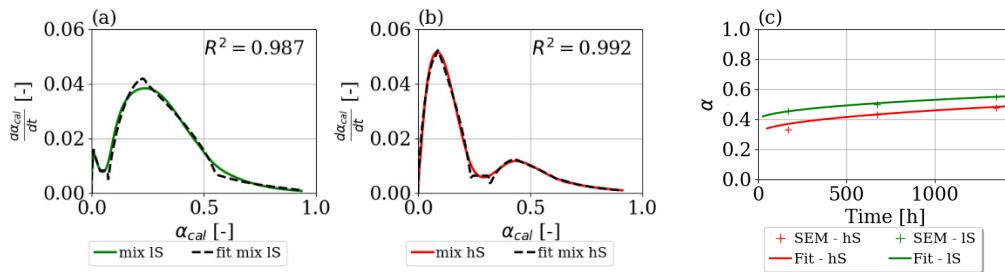


Figure 2. (a) and (b): Results of the modeling of calorimetry results for both mixes with single-particle models. (c) Results of SEM for both mixes.

The cumulative heat release of the mix IS is higher than the one of the mix hS. After seven days, the equivalent degree of reaction obtained with the use of equation (2) is equal to 93.4 % for the mix IS and 91.0 % for the mix hS. Nevertheless, these results must be rescaled with SEM results, which give the actual proportion of unreacted slag. The corresponding degrees of dissolution for the mix IS and the mix hS are equal to 45.5 % and 33.3 %, respectively. Both methods are complementary to predict the degree of dissolution of slag over time.

### 3.2 Reaction Products

Reaction products for both mixes are quite different. XRD results Figure 3 indicate the presence of C-A-S-H (29.5, 32 and 50°) and hydrotalcite (11.5, 23, 34, 39.5°) for the mix IS. These phases have already been identified in AAS systems (Haha *et al.* 2011). In comparison, the mix hS presents few crystallized phases. FTIR results are also displayed in Figure 3. The peaks at

3300  $\text{cm}^{-1}$  and 1650-1600  $\text{cm}^{-1}$  are attributed to O-H bending modes of water. The different peaks in the range [1200  $\text{cm}^{-1}$ ; 800  $\text{cm}^{-1}$ ] correspond to  $Q^n$  sites. For the mix IS,  $Q^2$ ,  $Q^1$  and  $Q^0$  sites are found at 1025  $\text{cm}^{-1}$ , 935  $\text{cm}^{-1}$  and 814  $\text{cm}^{-1}$  respectively. For the mix hS,  $Q^2$ ,  $Q^1$  and  $Q^0$  sites are found at 1947  $\text{cm}^{-1}$ , 943  $\text{cm}^{-1}$  and 835  $\text{cm}^{-1}$ . The shift to the right for the mix IS, meaning lower characteristic wavelengths for  $Q^n$  sites, is attributed to a greater aluminum uptake in the C-A-S-H structure (Clayden *et al.* 1999).

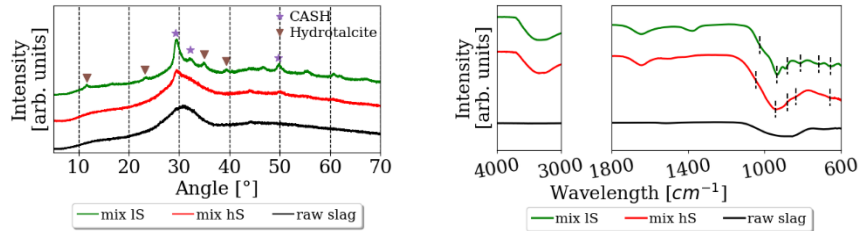


Figure 3. XRD (left) and FTIR (right) results at 28 days of both mixes.

DTG results of Figure 4 confirm the presence of C-A-S-H and hydrotalcite in the mix IS. They show also that the mix hS is composed of C-A-S-H. Finally, DTA results are shown in Figure 4. They show for the mix hS a peak at around 800 °C. This is representative of both C-A-S-H with a high Ca/Si ratio or magnesium silicate hydrates (M-S-H).

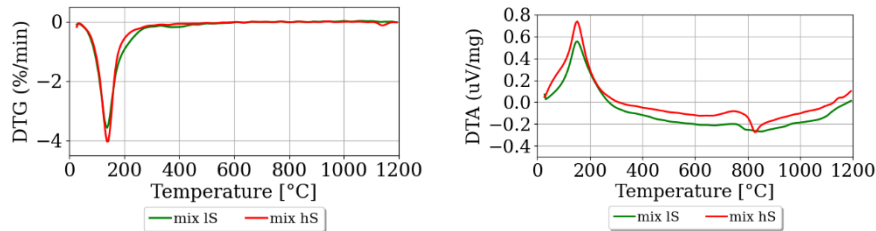


Figure 4. DTG (left) and DTA (right) results at 28 days for both mixes.

### 3.3 Flexural and Compressive Strength

The results of flexural and compressive strengths of paste samples are given in Figure 5. They show that both mixes present reasonable strengths in comparison to other cementitious systems (Topič *et al.* 2017). Compressive strength development of mix hS is a bit delayed in comparison to mix IS, in accordance with the kinetics of the reaction (see Figure 1). The drop in flexural strength at 28 days for the mix IS can be due to the relative high presence of cracks at that age in the AAS matrix caused by a higher shrinkage (Li *et al.* 2019). These results must be completed in the future by experiments on the concrete scale to validate the use of these both mixes for structural applications.

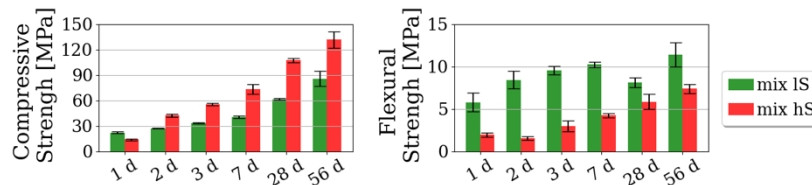


Figure 5. Compressive strength (left) and flexural strength (right) results for both mixes.

## 4 CONCLUSION

The kinetic reaction of AAS with sodium silicate can be modeled as the following succession of kinetically governed steps. Firstly, nucleation around the sodium silicate crystals present in the alkali solution and shrinking core process for the first peak. Then, a nucleation period modeled by a constant rate reaction is considered. A nucleation around the slag particle, shrinking core process and diffusion for the second acceleration period. Depending on the alkali solution, the relative importance of each acceleration period is modified and different products are formed, such as C-A-S-H and hydrotalcite. Sodium silicate activated slag shows sufficient compressive and flexural strengths even if kinetic and reaction products are quite different from OPC.

### Acknowledgments

The project leading to this application has received funding from the European Union's Horizon 2020 research and innovation programme under the Marie Skłodowska-Curie grant agreement No 813596.

### References

- Caron, R., Patel, R., and Dehn, F., *Activation Kinetic Model and Mechanisms for Alkali-Activated Slag Cements*, Construction and Building Materials, Mar, 2021.
- Clayden, N. J., Esposito, S., Aronne, A., and Pernice, P., *Solid State Al NMR and FTIR Study of Lanthanum Aluminosilicate Glasses*, Journal of Non-Crystalline Solids 258, Nov, 1999.
- DIN EN 196-1, *Prüfverfahren für Zement - Teil 1: Bestimmung der Festigkeit; Deutsche Fassung EN 196-1:2016*. Beuth Verlag, 2016.
- Fernández-Jiménez, A. and Puertas, F., *Structure of Calcium Silicate Hydrates Formed in Alkaline-Activated Slag: Influence of the Type of Alkaline Activator*. Journal of American Ceramic Society, 86, Aug, 2003.
- Gong, K. and White, C. E., *Impact of Chemical Variability of Ground Granulated Blast-Furnace Slag on the Phase Formation in Alkali-Activated Slag Pastes*, Cement and Concrete Research 89, Nov, 2016.
- Haha, M. B., Lothenbach, B., Le Saout, G., and Winnefeld, F., *Influence of Slag Chemistry on the Hydration of Alkali-Activated Blast-Furnace Slag — Part I: Effect of MgO*. CCR 41, Jan, 2011.
- Li, Z., Liu, H., and Guang, Y., *Drying Shrinkage of Alkali-Activated Slag and Fly Ash Concrete; A Comparative Study with Ordinary Portland Cement Concrete*, Heron 64, 2019.
- Lloyd, R. R., Provis, J. L., and van Deventer, J. S. J., *Microscopy and Microanalysis of Inorganic Polymer Cements. 2: The Gel Binder*, Journal of Materials Science 44, Jan, 2009.
- Myers, R. J., Bernal, S. A., Gehman, J. D., and van Deventer, J. S.J., Provis, J. L., *The Role of Al in Cross-Linking of Alkali-Activated Slag Cements*, Journal of the American Ceramic Society 98, Mar, 2015.
- Parrot, L. J., and Killoh, D. C., *Prediction of Cement Hydration*, British Ceramic Proceedings, 1984.
- Prentice, D. P., Bernal, S. A., Bankhead, M., Hayes, M., and Provis, J. L., *Phase Evolution of Slag-Rich Cementitious Grouts for Immobilisation of Nuclear Wastes*, Advances in Cement Research 30, Sep, 2018.
- Riding, K.A., Poole, J.L., Folliard, K.J., Juenger, M.C.G., and Schindler, A.K., *Modeling Hydration of Cementitious Systems*. ACI Materials Journal 109, 2012.
- Shi, C. and Day, R. L., *A Calorimetric Study of Early Hydration of Alkali-Slag Cements*. CCR 25, 1995.
- Topič, J., Fládr, J., and Prošek, Z., *Flexural and Compressive Strength of the Cement Paste with Recycled Concrete Powder*, Advanced Materials Research, 1144, 2017.
- Zhang, J. and Scherer, G. W., *Comparison of Methods for Arresting Hydration of Cement*, Cement and Concrete Research 41, Mar, 2011.